CHAPTER 10

Remote sensing signatures: Measurements, modelling and applications

Shunlin Liang, Michael Schaepman & Mathias Kneubühler

ABSTRACT: Signatures from five remote sensing domains—spectral, spatial, angular, temporal and polarization—provide the basis for the description and discrimination of Earth surfaces and their variability. These signatures have been used for a wide range of terrestrial applications. In this chapter, we review the measurements, modelling and applications of these signatures with emphasis on recent advances, and a focus mainly on optical remote sensing.

Keywords: Remote sensing, signature, spectral, spatial, angular, temporal, polarization

10.1 INRODUCTION

The radiation signals (*L*) received by a remote sensor can be generally represented mathematically as follows:

$$L = f(\lambda, A, t, \Theta, p, \Psi_a, \Psi_s) \qquad (1)$$

where λ indicates spectral dependence; *A* refers to the spatial context and *t* the temporal variations; Θ represents the angles specifying the illumination viewing geometry and *p* the degree to which the radiation is polarized; Ψ_a and Ψ_s represent the parameter set describing the atmosphere and the land surface, respectively.

One of the most important objectives of terrestrial remote sensing is to estimate surface properties (Ψ_s) from radiation signals (*L*) at specific spectral bands, spatial and temporal resolutions, viewing geometry and polarization states. These five domains (spectral, spatial, angular, temporal and polarization) are denoted as remote sensing signatures (Gerstl 1990).

In the following, we review recent advances in acquisition and use of these five signatures in the aspects of measurements, modelling, inversion and applications. Although these signatures are discussed separately, they are ultimately measured, modelled and utilized in combination for the most part. Worldwide conferences, such as the "International Symposium on Physical Measurements and Signatures in Remote Sensing"

(2005, China; 2007, Switzerland), organized by us on behalf of the ISPRS Commission VII Working Group 1, reflect the research involving multiple signatures.

10.2 SPECTRAL SIGNATURES

For any given object on the land surface, the amount of solar radiation that is reflected or emitted varies with wavelength. The spectral signatures are the radiation signals collected at different spectral bands that form the basis to classify land surfaces and/or evaluate their geophysical and biophysical properties.

10.2.1 *Measurements*

The spectral properties of land surfaces are measured by either multispectral or hyperspectral sensor systems depending on the number and spectral width of bands. Table 10.1 shows the multispectral bands of some typical moderate resolution imaging radiometers.

Hyperspectral imagers typically acquire hundreds of contiguous spectral bands throughout the visible to thermal infrared spectrum. Multispectral signatures are discrete compared to the contiguous signatures obtained from hyperspectral images. Widely used hyperspectral imagers include the airborne AVIRIS, CASI, AISA and Hymap, as well as the satellite-based Hyperion and CHRIS employed mainly for terrestrial applications.

Table 10.1. Some of the principal sensors useful for terrestrial moderate resolution remote sensing, revised from Townshend & Justice (2002).

Sensor	Platform	Spatial resolution (m)	Swath (km)	Spectral bands (nm)
AATSR	ERS-2	1000	500	480–500
				540–560
				630–690
				795–835
				1550–1700
AVHRR	NOAA–POES	1100	2700	580–680
				725–1000
				1580–1640
				3550–3930
				10,300–11,300
				11,500–12,500
MERIS	Envisat	300	575	660–670
		1200	1150	855–875
MODIS	Terra and Aqua	500		459–479
		500		545–565
		250		620–670
		250		841–876
		500		1230–1250
		500		1628–1652
		500		2105–2155
		1000		3929–3989
		1000		10,780–11,280
		1000		11,770–12,270
POLDER	ADEOS	6000	2400	433–453
				555–575
				660–680
				845–885
SeaWiFs	OrbView2/Sea Star	1100	2800	443–453
		4500		545–565
				660–680
				845–885

Microwave remote sensing uses several wavelengths, which were given code letters during World War II and which remain unchanged to this day (Table 10.2).

Lidar remote sensing relies on active laser systems operating at several wavelengths. Topographic mapping and vegetation monitoring Lidars generally use 1064 nm lasers, while bathymetric systems typically use 532 nm frequency lasers due to the ability of this frequency to penetrate water with less attenuation.

10.2.2 *Modelling*

Spectral signatures can be modelled using three methods: radiative transfer (RT), geometric-optical (GO), and computer simulations. The distinction between RT and GO models is becoming increasingly blurred because hybrid models that integrate RT and GO models have been developed. Computer simulation models require extensive computer resources and processing time and are appropriate for surface radiation simulations. The basic principles and representative models have been discussed by Liang (2004) and different authors of the special issue of Remote Sensing Reviews (Liang & Strahler 2000), and recent advances are reviewed below.

The development of new radiative transfer models has slowed significantly in recent years. An exhaustive review of existing literature resulted in only a few publications describing new RT models in a wide variety of fields. For example, Pitman et al. (2005) applied a numerical RT algorithm to calculate quartz emissivity. Kokhanovsky et al. (2005) developed an approximate snow reflectance model based on the asymptotic solution to the RT equation. Li & Zhou (2004) simulated the snow-surface bidirectional reflectance factor

Table 10.2.   Microwave sensor band codes.

Band	Frequency (GHz)	Wavelength (cm)	System applications
Ka	40–26	0.8–1.1	Early airborne radar systems
K	26.5–18.5	1.1–1.7	Early airborne radar systems
X	12.5–8	2.4–3.8	Extensively on airborne systems for military reconnaissance and terrain mapping
C	8–4	3.8–7.5	Common on many airborne research systems (NASA AirSAR) and spaceborne systems (including ERS-1 and 2 and RADARSAT).
L	2–1	15.0–30.0	Used onboard American SEASAT and Japanese JERS-1 satellites and NASA airborne system
P	1–0.3	30.0–100.0	Longest radar wavelengths, used on NASA experimental airborne research system

(BRF) and hemispherical directional reflectance factor (HDRF) of snow-covered sea ice multilayered azimuth- and zenith-dependent plane-parallel RT model.

In the field of vegetation canopy studies, recent efforts are mainly focused on determining the three-dimensional (3-D) structure of the canopy using one-dimensional (1-D) models (Pinty et al. 2004a, Rautiainen & Stenberg 2005, Smolander & Stenberg 2003, Widlowski et al. 2005) or stochastic radiative transfer models (Kotchenova et al. 2003, Shabanov et al. 2005). Liangrocapart & Petrou (2002) developed a two-layer model of the bidirectional reflectance of homogeneous vegetation canopies, taking into account the anisotropic scattering of both the vegetation canopy and the background, such as bare soil or leaf litter. Community efforts to compare some vegetation radiative transfer models are ongoing (Pinty et al. 2004b, Widlowski et al. 2007). Nilson et al. (2003) demonstrated the possible applications of a multipurpose forest reflectance model. Combining leaf radiative transfer models with canopy scale models in various permutations has become more popular and is increasingly used in scaling based approaches (e.g. PROSPECT/GeoSAIL, PROSPECT/FLIGHT in Koetz et al. (2004); PROSPECT/DART (Malenovsky et al. 2008); and other coupled approaches in Bacour et al. (2002)).

The classic GO models essentially characterize the interaction of direct solar radiation with land surfaces. Including the diffuse radiation field in the GO model leads to a hybrid RT/GO model (Peddle et al. 2004). GO models have been used recently for classifying forest types and estimating biophysical parameters (Peddle et al. 2004) and detecting forest structural change (Peddle et al. 2003, Zeng et al. 2008b) from Thematic Mapper (TM) imagery, modelling soil reflectance (Cierniewski et al. 2004), determining the gap fraction of forest canopy (Liu et al. 2004), and estimating woody plant coverage of the grasslands (Chopping et al. 2006), and background reflectance (Canisius & Chen 2007) from multiangular observations. The same principle has also been used for topographic correction of remote sensing imagery in forested terrain (Soenen et al. 2005).

Little progress has been made in developing computer simulation models (e.g. radiosity, Monte Carlo ray tracing), but several studies recently use this approach. For example, Casa & Jones (2005) estimated potato crop biophysical parameters using a look-up table (LUT) created from a ray tracer. Börner et al. (2001) developed an end-to-end multispectral and hyperspectral simulation tool based on the ray tracing principle. Ray-tracing methods have been used to simulate both optical and microwave signatures (Disney et al. 2006) and to estimate forest structural parameters (Kobayashi et al. 2007).

10.2.3   *Signature generation and applications*

The subset of the spectral signatures generated from a set of measurements at different wavebands is usually more valuable for specific applications. Colour compositing using two or three bands for visual interpretation is the classic example. Many quantitative models or image classifications are normally based on a few bands or their combinations. The linear transformation techniques include principal component transformation and Tasselled Cap transformation.

More popular methods are based on vegetation indices (VI). Earlier developed indices have been extensively summarized by Liang (2004). Numerous new indices have been put forth. A comprehensive analysis of broadband and narrowband vegetation indices and their angular sensitivity is described in Verrelst et al. (2008). A brief description of some of these algorithms follows. Gitelson et al. (2003) compared a series of indices and found the following three perform very well:

$$(R_{800} - R_{700})/(R_{800} + R_{700}), \quad R_{860}/(R_{708} * R_{550})$$
$$\text{and } R_{750\text{-}800}/R_{695\text{-}740} - 1 \tag{1}$$

The last index is linearly related to chlorophyll concentrations. Ustin et al. (2008) compared the retrieval capacity of indices and models for the plant pigment system. In a recent study estimating leaf area index (LAI) and crown volume (VOL), Schlerf et al. (2005) demonstrated that linear regression models quantify LAI and VOL accurately using hyperspectral image data. Harris et al. (2005) used the floating-position water band index to estimate leaf water moisture. To assess the water content of vegetation, they also compare leaf water moisture to the normalized difference water index (NDWI) and the moisture stress index (MSI). The normalized difference snow index (NDSI) is an indicator of snow cover (Salomonson & Appel 2004). Chen et al. (2005b) developed a biological soil crust index (BSCI) that exaggerates the difference between biological soil crusts and bare sand, dry plant material or green plant backgrounds. Chikhaoui et al. (2005) proposed a "land degradation" index to characterize land degradation in a small Mediterranean watershed using Advanced Spaceborne Thermal Emission and Reflection Radiometer (ASTER) data and ground-based spectro-radiometric measurements.

Although the conventional multivariate regression analyses using spectral signatures are widely used, different machine learning methods and other advanced statistical analysis techniques show great potential, such as artificial neural network (ANN) methods for estimating various biophysical variables (Fang & Liang 2003, 2005); genetic algorithms for estimating LAI (Fang et al. 2003), regression tree methods for estimating fractional vegetation coverage (Hansen et al. 2002), Bayesian networks for estimating LAI (Kalacska et al. 2005), and support vector machines for estimating LAI from multiangular observations (Durbha et al. 2007).

Use of spectral signatures via physical reflectance or emittance models (see Section 2.2) and optimization methods has been popular recently in terrestrial remote sensing. For example, Gascon et al. (2004) estimated LAI, crown coverage and leaf chlorophyll concentration from SPOT and IKONOS imagery using a 3-D canopy radiative transfer model. To reduce computational requirements, some parametric functions are determined using LUTs created by the 3-D reflectance model. Meroni et al. (2004) applied this algorithm to invert LAI from hyperspectral data. Schaepman et al. (2005) inverted biophysical and biochemical variables from multiangular and hyperspectral remote sensing data using a coupled leaf-canopy-atmosphere radiative transfer model. The multiangle imaging spectroradiometer (MISR)

science team also used this method to produce land surface products (Diner et al. 2005). Qin et al. (2008) incorporated the adjoint algorithm of the canopy RT model in the optimization process to speed up computation.

The high computational demands of the optimization approach have led to the use of simpler surface reflectance models rather than forcing optimization algorithm efficiencies. One of the general trends in terrestrial remote sensing is to use simpler empirical or semi-empirical models. The optimization algorithms are used to estimate the parameters in these simple models. The parameters are then related to surface properties. For example, Widlowski et al. (2004) fitted a simple BRDF model to multiangular observations and then linked the surface structural properties to one of the parameters. Chen et al. (2005c) used this approach to map the global clumping index from multiangular observations.

An alternative solution to overcome the high computational demand problem is to use the LUT approach, which has been used for a variety of remote sensing inversion issues, such as atmospheric correction (Liang et al. 2006b), estimating LAI (Koetza et al. 2005) and incident solar radiation (Liang et al. 2006a). In an ordinary LUT approach, the dimensions of the table must be large enough to achieve high accuracy, which leads to much slower on-line searching. Moreover, many parameters must be fixed in the LUT method. To reduce the dimensions of the LUTs for rapid table searching, Gastellu-Etchegorry et al. (2003) developed empirical functions to fit the LUT values so that a table searching procedure becomes a simple calculation of the local functions. Alternatively, Liang et al. (2005) developed a simple linear regression instead of table searching for each angular bin in the solar illumination and sensor viewing geometry. Dorigo et al. (2007) gave an overview of models and LUT optimization techniques used in agro-ecosystem modelling.

Spectral signatures have been used to estimate atmospheric aerosol loadings and water vapour contents that are especially important for atmospheric correction of optical remote sensing imagery. The differential absorption technique is widely used to estimate the total water vapour content of the atmosphere directly from multispectral or hyperspectral imaging systems. The general idea is to utilize one spectral band in the water absorption region (e.g. 0.94 μm) and one or more bands outside of the absorption region. In a recent study, Liang & Fang (2004) applied an ANN to estimate water vapour from hyperspectral data. Miesch et al. (2005) developed a water vapour correction algorithm for hyperspectral data using Monte Carlo simulations. A relatively long history exists for estimating aerosol loadings from remotely sensed imagery using the spectral signatures such as

the "dark-object" methods (e.g. Hsu et al. 2004, Liang et al. 1997) and the hyperspectral method (Liang & Fang 2004);

10.3 SPATIAL SIGNATURES

Land surface information is acquired by sensors at different spatial resolutions, which are usually characterized by the pixel size on the ground. Spatial resolution is sometimes expressed in terms of Instantaneous Field of View (IFOV). The spatial signature depends on the spatial resolution of the sensor and its spatial response in addition to the surface variations. Generally speaking, the coarser the spatial resolution, the less variation there is between pixels in the image (Curran 2001, Jupp et al. 1988, 1989, Woodcock & Strahler 1987).

10.3.1 *Measurements*

Current remote sensing data are of different spatial resolutions, such as ultra resolution (e.g. Quick-Bird, Ikonos), fine resolution (e.g. ETM+, ASTER), medium resolution (e.g. MODIS, MERIS) and coarse resolution. The microwave sensors are also providing finer spatial resolutions from kilometres to metres (Table 10.3).

10.3.2 *Modelling*

Spatial signatures characterize the spatial dependencies of pixel values, which are generally spatially autocorrelated, non-stationary, non-normal, irregularly spaced and discontinuous. Different methods can be used to model and characterize these spatial signatures and we discuss a few typical methods. Although there are also many other methods such as the Moran's I spatial autocorrelation metric for coral reef study (Purkis et al. 2006), lacunarity methods and fractal triangular prisms for classifying urban images (Myint & Lam 2005), they are not addressed here. Additional details are available elsewhere (Lam 2008).

10.3.2.1 *Geo-statistics*
Geo-statistics, as part of spatial statistics, have been widely employed in remote sensing (e.g. Bailey & Gatrell 1995, Cressie 1993, Curran 1988, Goovaerts 1997, Woodcock et al. 1988a, 1988b). The typical geo-statistical measures may include: (i) variogram, (ii) covariance function, (iii) correlogram, (iv) general relative variogram, (v) pairwise relative variogram, (vi) rodogram, and (vii) madogram. Combining GO models with geo-statisitcal methods such as regression kriging or annotated co-kriging substantially improves the elimination of model imperfections and allows the production of spatially continuous information (Zeng et al. 2008a).

10.3.2.2 *Grey level co-occurrence matrix*
Co-occurrence measures use a grey tone spatial dependence matrix to calculate texture values of the image. This is a matrix of relative frequencies in which pixel values occur in two neighbouring processing windows separated by a specified distance and direction. It shows the number of occurrences of the relationship between a pixel and its specified neighbour. This type of spatial structure information is particularly useful for high resolution images.

Table 10.3. Characteristics of some typical microwave sensors, adapted from Shi (2008).

Sensor	Frequency in GHz	Polarization	Incidence In degree	Pixel Resolution in m	Available Time Frame
ERS-1/2	5.3	VV	Fixed at 23º	3.8 to 12.5	Since 1991/1995
ASAR	5.33	Dual-polarization	varying with mode	3.8 to 150	Since 2002
Radarsat-1	5.3	HH	varying with mode	10 to 100	Since 1997
SIR-C/X-SAR	1.25 and 5.3/9.6	Fully polarimetric/VV	varying with data takes	6 to 27	April and October, 1994
JERS-1	1.27	HH	Fixed at 35°	18	1994–1997
PALSAR	1.27	Fully polarimetric, Dual-polarization, and HH	varying with mode	10 to 100	Since Dec. 2005
Radarsat-2	5.3	Fully polarimetric, Dual-polarization, and HH	Varying with mode	3 to 100	2006
Terral-SAR	9.6	VV or Dual-polarization	Varying with mode	1 to 16	2006

Many investigations consider the use of the grey level co-occurrence probability texture features for classification purposes only (Jobanputra & Clausi 2006).

10.3.2.3 *Fourier transformation*
Power spectrum analysis is useful for those images that have regular wave patterns with a constant interval, such as wave patterns of sand dunes. Fourier transformation is applied to determine the power spectrum, which gives the frequency and direction of the pattern. Fourier transformations are typically used for the removal of noise such as striping, spots, or vibration in imagery by identifying periodicities (areas of high spatial frequency).

10.3.2.4 *Wavelet transform*
The wavelet transform can be effectively used as a spatial analysis tool for modelling spatial relationships of remote sensing data. Wavelet analysis is a technique to transform an array of N numbers from their actual numerical values to an array of N wavelet coefficients.

Since the wavelet functions are compact, the wavelet coefficients measure only the variations around a small region of the image data. This property makes wavelet analysis very useful for image processing; the "localized" nature of the wavelet transform allows easy identification of features in the image data such as spikes (e.g. noise or discontinuities), discrete objects, edges of objects, etc. The localization also implies that a wavelet coefficient at one location is not affected by the coefficients at another location in the data. This makes it possible to remove "noise" of all different scales from a signal, simply by discarding the lowest wavelet coefficients.

10.3.2.5 *Markov random field models*
A Markov random field (MRF) is recognized as a powerful stochastic tool to model the joint probability distribution of image pixels in terms of local spatial interactions. A wide range of MRF models have been proposed over the last several decades. Essentially, an MRF model considers an image as a realization of a Markov random field, and is often parameterized by a function, consisting of two basic components: observable variables and model parameters. MRF models can be used not only to extract texture features from image textures but also to model the image segmentation problem. Multiresolution spatial models or approximate kriging methods have been adapted recently to handle massive data sets for imputation and smoothing (Magnussen et al. 2007).

10.3.2.6 *Spatial scaling*
Merging images of different spatial and spectral resolutions to create a high spatial resolution multispectral combination is considered a spatial scaling process. Various approaches have been proposed to integrate image data with different spatial resolutions (Pohl & van Genderen 1998, Ranchin et al. 2003, Vesteinsson et al. 2008).

Spectral (un)mixing is an algorithm that estimates the percentage of each land cover (called endmembers) within each low resolution multi- and hyperspectral pixel (Asner & Lobell 2000, Gross & Schott 1998), which is considered as a spatial downscaling problem. Here we do not attempt to distinguish subpixel mapping, unmixing, or soft classification. Recent developments include unmixing with variable endmembers (Garcia-Haro et al. 2005), the directional mixing method (Garcia-Haro et al. 2006), stochastic mixing model for hyperspectral imagery (Eismann & Hardie 2004, 2005), unmixing using neural networks and wavelets (Mertens et al. 2004) and genetic algorithms (Mertens et al. 2003).

10.3.3 *Applications*
Geo-statistics has been widely applied in quantitative remote sensing (Curran & Atkinson 1998), such as in studying the structure and understanding the nature of spatial variation in remote sensing images (Woodcock et al. 1988b, Ramstein & Raffy 1989); in forestry to analyse forest stand structure (Cohen et al. 1990, St-Onge & Cavayas 1995); in the estimation of structural damage in balsam fir stands (Franklin & Turner 1992); in the sampling of ground data that is to be correlated with remotely sensed data (Atkinson & Emery 1999); and in estimating biomass (Phinn et al. 1996).

Wavelet transformation has been used for image classification (Kandaswamy et al. 2005, Meher et al. 2007, Schmidt et al. 2007), segmentation (De Grandi et al. 2007), compression (Li et al. 2007), noise removal (Chen et al. 2006b), and fusion (Amolins et al. 2007).

Random field models have been used for identifying urban areas from optical imagery (Zhong & Wang 2007), image classification (Luo et al. 2007) and segmentation (Xia et al. 2006), and spatial-temporal urban landscape change analysis using a Markov chain model and the genetic algorithm (Tang et al. 2007).

The spatial co-occurrence matrix has been used for evaluating land development (Unsalan 2007), estimating forest structure variables (Kayitakire et al. 2006), predicting population density (Liu et al. 2006), and discriminating urban features (Myint et al. 2004, Zhang et al. 2003).

Boucher et al. (2006) presented a method that exploits both the temporal and spatial domains of time series satellite data to map land cover changes.

10.4 ANGULAR SIGNATURES

Many spaceborne sensors can observe earth surfaces off-nadir in order to increase swath width and temporal resolution, and to exploit angular variations in the reflectance of various land surfaces. Angular signatures are the observations of surfaces illuminated and measured at different directions. They may be considered as noise in calculating the vegetation indices, for example, and we need to remove the angular dependence. On the other hand, angular signatures can be extremely valuable for estimating land surface variables.

10.4.1 *Measurements*

The spaceborne sensors for near-simultaneous multi-angular acquisition include the NASA MISR flown on the NASA Earth Observing System Terra; the French Space Agency's (CNES) POLarization and Directionality of the Earth's Reflectance (POLDER), flown initially on the Japanese ADEOS satellite series and currently on the CNES Parasol platform; and Sira (UK) Ltd.'s Compact High Resolution Imaging Spectrometer (CHRIS), flown on the European Space Agency (ESA) Proba-1 satellite. Terra was launched in December 1999, Proba in 2001 and Parasol in 2004.

To perform nearly simultaneous observations from space at multiple view angles, two technical solutions may be used: a) multiple optics or b) accurate along track pointing. The Along Track Scanning Radiometer 1 (ATSR-1) flown on ERS-1 was based on solution (a). ATSR-1 was followed by ATSR-2 in 1995 and the Advanced ATSR (AATSR) on ENVISAT in 2001. All ATSR sensors acquire dual-view angle data (approximately 0° and 53° at surface) in four spectral channels for ATSR-1 and seven spectral channels for ATSR-2 and AATSR. The use of the along track scanning technique makes it possible to observe the same point on the Earth's surface at two view angles through two different atmospheric paths within a short period of time.

Multiangular data sets can be acquired sequentially rather than near-simultaneously, and work with these accumulating, or "sequential", systems is also making important contributions to multiangle remote sensing.

10.4.2 *Modelling, inversion and applications*

The basic modelling methods are very similar to those described in Section 2.2, and the inversion methods focus mainly on physical approaches. The recent paper by Diner et al. (2005) in terms of MISR and three review papers on the optical and thermal multi-angular remote sensing (Schaepman 2007, Chopping 2008, Menenti et al. 2008) provide comprehensive

discussions. Angular reflectance terminology has seen further standardization efforts, resulting in a comprehensive overview of multiangular data products (Schaepman-Strub et al. 2006). In the following, only a few application examples are introduced.

Angular signatures have been used to estimate aerosol properties (Grey et al. 2006, Martonchik et al. 2002), fractional vegetation coverage (North 2002, Roujean & Lacaze 2002), LAI and FPAR (Casa & Jones 2005, North 2002, Qi et al. 2000, Roujean & Breon 1995, Zhang et al. 2000), canopy clumping index (Chen et al. 2005c), biochemical parameters (Kimes et al. 2002, Kuusk 1998), surface albedo (Schaaf et al. 2008), and land surface skin temperature and emissivity (Coll et al. 2006, Jimenez-Munoz & Sobrino 2007, Menenti et al. 2008, Sobrino et al. 2004).

There are additional studies combining angular signatures with other signature types (Baret & Buis 2008). For example, Kimes et al. (2006) estimated forest structural data from the airborne Laser Vegetation Imaging Sensor and Airborne MISR (AirMISR). Kneubühler et al. (2006) assessed the spectral behaviour of agricultural crop stands using multitemporal angular CHRIS/PROBA data. In fact, angular signatures are almost always combined with spectral signatures (Diner et al. 2005).

10.5 TEMPORAL SIGNATURES

Temporal signatures are derived from time sequences of observations. They are particularly significant for monitoring the Earth's environmental changes.

10.5.1 *Measurements*

The measurement of temporal signatures is synonymous with temporal resolution and other related terms, such as the "repeat" cycle or "revisit time". Temporal resolution depends on various other factors, including the satellite's orbital altitude and the sensor's view angle (which together influence the image's area of coverage, or swath width), the instrument's tilting capabilities and the latitude of the area of interest (Aplin 2006).

The current and planned Landsat-type satellites cover the complete equatorial surface during each orbital repeat cycle by having ground swaths between 120 and 200 kilometres. Their orbital periods, and thus global coverage times, vary from 16 days for Landsat to 22, 24 and 26 days for the Indian, French and Chinese/Brazilian satellites. Taken singly, even these repeat cycles are too long for many applications. The moderate resolution satellites (Table 10.1) have much higher temporal resolutions, typically daily. For
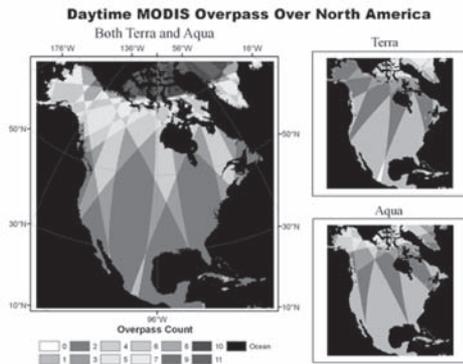
Figure 10.1. Number of MODIS overpass counts over North America based on the Terra and Aqua orbital simulation from GMT 12:00 to 24:00, 16 June 2006 (Wang et al. 2008). (see colour plate page 493)

MODIS, the temporal resolutions, which depend on the geographic location, are shown in Figure 10.1.

To monitor the temporal variations of the dynamic atmospheric system for accurate weather and climate prediction, geo-stationary satellites are operational in geo-stationary orbits and are also useful for land environmental monitoring. The imaging sensors acquire data typically every 15–30 minutes.

10.5.2 *Modelling*

Before reviewing the modelling techniques, it is helpful to discuss three pre-processing techniques, namely, temporal compositing, temporal smoothing, and gap filling.

10.5.2.1 *Temporal compositing*
One of the most common techniques used to obtain cloud-free and spatially coherent images is temporal compositing (Cihlar et al. 1994, Holben 1986). Compositing is a technique that for any given pixel selects the date that best fits a given criterion, for a pre-specified period of time.

The first compositing algorithm developed and most commonly used is the normalized difference vegetation index (NDVI) maximum value composite (Holben 1986). Several other compositing algorithms have been studied, including the Soil Adjusted Vegetation Index (SAVI) maximum value composite (Qi & Kerr 1997), minimum value composite of the red band; NDVI maximum value composite followed by the minimum value of the viewing zenith angle (Cihlar et al. 1994). Cabral et al. (2003) compared five different algorithms using vegetation data, including maximization of NDVI, minimization of the red channel, maximization of NDVI followed by

minimization of short-wave infrared, the third lowest value of near-infrared, and the third lowest darkness value (defined as the arithmetic mean of the red and NIR bands). Selection of the third lowest values is based on the assumption that there is a low likelihood of a cloud shadow falling on a given pixel more than twice, over a period of one month.

10.5.2.2 *Temporal smoothing*
Temporal compositing is a simple approach, but if the composite period is long, the land surface does not remain static; and if it is too short, the atmospheric disturbance cannot be removed effectively, especially in cloudy regions. For example, there exist many low quality pixels in 8- or 16-day composite MODIS products (Moody et al. 2005). Several methods, based on interpolation of time series data, have been proposed to remove such noise and to reconstruct high quality NDVI time-series data. These methods can be generally categorized into two types. The first type includes removing noise in the time domain, such as the best index slope extraction (BISE) algorithm (Viovy et al. 1992), the asymmetric Gaussian function fitting approach (Jonsson & Eklundh 2002), the weighted least squares linear regression approach (Sellers et al. 1994), the Savitzky-Golay filter approach (Chen et al. 2005a) and the ecosystem-dependent temporal interpolation technique (Moody et al. 2005). The second type includes noise removal methods in the frequency domain, such as Fourier-based fitting methods (Roerink et al. 2000).

Lu et al. (2007) applied a wavelet-based method to remove the contaminated data from MODIS NDVI, LAI and albedo time-series, with a comparison with the BISE algorithm, Fourier-based fitting method, and the Savitzky-Golay filter method.

10.5.2.3 *Gap filling*
Many space agencies (e.g. NASA) are routinely producing high-level land products, which are usually spatially and temporally discontinuous due to cloud cover, seasonal snow and instrument problems. To enable these products to be used with their various kinds of gaps, it is intuitively appealing to use either temporal or spatial filters. Several mathematical filters have been used to fill gaps in remotely sensed data, such as simple linear interpolation, BISE (Viovy et al. 1992), Fourier transformation (Hermance 2007, Julien et al. 2006, Roerink et al. 2000), Asymmetric Gaussian filter (Jonsson & Eklundh 2002), Savitzky-Golay filter (Chen et al. 2005a), or locally adjusted cubic-spline capping method (Chen et al. 2006a). These methods have been used mainly to restore the NDVI profile (Cihlar 1996, Sellers et al. 1994), but they can also be used for LAI with some adjustments.

Moody et al. (2005) tried to combine both temporal and spatial methods and developed an ecosystem-dependent temporal interpolation technique to fill missing or snow-covered pixels in the MODIS albedo data product. Fang et al. (2007, 2008) have developed a data filtering algorithm, called the temporal spatial filter (TSF), which integrates both spatial and temporal characteristics for different plant functional types.

10.5.2.4 *Functional representation*

Fisher (1994a,b) described the NDVI temporal profile using an empirical statistical model for agriculture crops, each crop corresponding to a set of coefficients. The formula is a double logistic function with five coefficients (k, c, p, d, q) and two constant values (*vb* and *ve*):

$$NDVI(t) = vb + \frac{k}{1 + \exp[-c(t - p)]} - \frac{k + vb - ve}{1 + \exp[-d(t - q)]} \tag{2}$$

where t is the time variable representing the day of the year, January 1 is set zero, k is related to the asymptotic value of NDVI, c and d (day^{-1}) denote the slopes at the first and second inflection points, p and q (day) are the dates of these two points, *vb* and *ve* are the NDVI values at the beginning and the end of the growing season. This function was used to decompose the temporal NDVI profile of a mixed pixel into the temporal NDVI profiles of several specific covers within the mixed pixel.

The temporal profiles of NDVI from AVHRR have also been presented by the classic Fourier function:

$$NDVI(t) = a_0 + \sum_{i=1}^{I} \left[a_i \cos\left(\frac{2\pi i}{T} t\right) + b_i \sin\left(\frac{2\pi i}{T} t\right) \right] \tag{3}$$

where T is the period of record. The low-order finite Fourier series has been used for classifying land surface cover types (Liang 2001).

A simplified version has been used for smoothing NOAA NDVI data (Hermance et al. 2007, Jonsson & Eklundh 2004):

$$\begin{aligned} f(t) &= c_1 + c_{2+}t + c_3 t^2 + c_4 \sin(\omega t) + c_5 \cos(\omega t) \\ &\quad + c_6 \sin(2\omega t) + c_7 \cos(2\omega t) \\ &\quad + c_8 \sin(3\omega t) + c_9 \cos(3\omega t) \end{aligned} \tag{4}$$

where $\omega = 6\pi / N$.

Another representation is the modified double-Gaussian curve

$$f(t) = A_1 e^{-(t - t_{01})/\Delta t_1} + A_2 e^{-(t - t_{02})/\Delta t_2} + a \cdot t + b \tag{5}$$

where the $(a \cdot t + b)$ is the "soil line" with parameters *a* and *b*.

10.5.3 *Applications*

Land surface change detection has to rely largely on the temporal signatures and some of the references can be found in the recent review papers (Coppin et al. 2004, Lam 2008).

These data smoothing approaches have also been utilized in a variety of other applications. The BISE algorithm has been used to classify vegetation and forest types (Xiao et al. 2003). The Fourier-based fitting approach has been employed to derive terrestrial biophysical parameters (Moody & Johnson 2001). Vegetation seasonality information has been extracted by use of Asymmetric Gaussian function fitting methods (Jonsson & Eklundh 2002). The ecosystem-dependent, temporal-interpolation technique can provide researchers with a snow-free, land-surface albedo product (Moody et al. 2005). Koetz et al. (2007) used multi-temporal CHRIS/PROBA data for LAI estimation based on an RTM inversion approach. The temporal signatures from the polar orbiting satellite data have been used recently for estimating aerosol optical depth (Liang et al. 2006b, Zhong et al. 2007) and incident solar radiation (Liang et al. 2006a, Liang et al. 2007).

Before finishing this section, we have to mention the terrestrial applications of temporal signatures from geo-stationary satellite data, including mapping surface albedos (Govaerts & Lattanzio 2007, Govaerts et al. 2004, Wang et al. 2007), land surface skin temperature (Oku & Ishikawa 2004, Sun et al. 2004), and solar radiation (Pinker et al. 2007, Wang et al. 2007, Zheng et al. 2007).

10.6 POLARIZATION SIGNATURES

Polarization is the property of electromagnetic waves that describes the direction of the electric field and is used to distinguish between the different directions of oscillation of electromagnetic waves propagating in the same direction. Polarization by scattering is observed as light passes through the atmosphere. Solar light reflected by natural surfaces is partly polarized. The surface polarized reflectance is highly anisotropic, and varies between zero close to the backscattering direction and a few per cent in the forward scattering direction. For a given observation geometry, the polarization is about twice as large over the pixels classified as "desert" as those over vegetated surfaces.

Polarization signatures represent the vector nature of the optical field across a scene. While the spectral signature is more about surface inherent properties, polarization signature tells us about surface features, shape, shading and roughness. Polarization tends to provide information that is largely uncorrelated with spectral and intensity images, and thus has the potential to enhance many fields of optical metrology.

An earlier review of the understanding and prospects of using polarized light was given by Herman & Vanderbilt (1997).

10.6.1 *Measurements*

In outdoor measurements, the most rapid variations of polarization with wavelength result from atmospheric spectral features. In the visible to shortwave-IR spectrum, there is strong variation with atmospheric aerosol content.

Polarized reflectance measurements have been made in the laboratory (Talmage & Curran 1986), at the surface (Breon et al. 1995a, Shibayama & Watanabe 2007), and from aircraft (Deuze et al. 1993) and space from POLDER. Despite the short life of the POLDER instrument, a unique set of observations on the global distribution of polarized reflectance was obtained. In addition to its multispectral and multidirectional capabilities, the POLDER radiometer is able to measure the polarization status of the reflected light at three wavelengths (443, 670 and 865 nm).

Before the launch of the ADEOS platform, the only spaceborne measurements of the polarized light reflected by the Earth were acquired using a photographic device from the space shuttle (Egan et al. 1991, Roger et al. 1994).

Polarization signatures are extremely valuable in microwave remote sensing. Horizontal polarization is much more sensitive to changes in the soil dielectric constant than vertical polarization measurements and information on the polarization difference has been used to characterize the vegetation in several studies and algorithms (Jackson 2008). The RADAR systems have evolved from single polarization to multi-polarization (Shi 2008), as shown in Table 10.3.

Polarization is also useful in Lidar remote sensing. For example, the presence of significant cross-polarized light relative to a linearly polarized transmitter can indicate the presence of ice in clouds or non-spherically shaped dust particles in the atmosphere. Polarized Lidars have been developed to measure Stokes parameters of backscattered light in studies of forest and Earth surface properties, and to enhance contrast in the Lidar detection of fish (Tyo et al. 2006).

10.6.2 *Modelling*

Modelling of polarization signatures is mainly based on radiative transfer theory in the vector form. Many publically available RT codes are in the vector format. A widely used radiative transfer code (6S) in optical remote sensing has a vector version now (Kotchenova & Vermote 2007, Kotchenova et al. 2006).

It is believed that polarized light is generated at the surface by specular reflection on the leaf surfaces or the soil facets. This hypothesis has been used to elaborate analytical models for the polarized reflectance of vegetation (Rondeaux & Herman 1991, Vanderbilt & Grant 1985) and bare soils (Breon et al. 1995b). For example, Nadal & Breon (1999) developed a simple polarized reflectance function to fit the POLDER data:

$$R_p(\theta_s, \theta_v, \varphi) = \rho \left[1 - \exp\left(-\beta \frac{F_p(\alpha)}{\mu_s + \mu_v} \right) \right] \qquad (6)$$

where $F_p(\alpha)$ is the specular reflectance of the Fresnel equation with the incident angle α, ρ and β are two parameters to be adjusted on the measurements for each cover type. ρ is the "saturation" value, whereas $\rho\beta$ is the slope of the linear relationship toward the large scattering angles. θ_s ($\mu_s = \cos(\theta_s)$) and θ_v ($\mu_v = \cos(\theta_v)$) are the solar and viewing zenith angles, φ is the relative azimuth angle between the solar illumination and viewing directions.

10.6.3 *Applications*

Polarization signatures can be treated as noise or signal. For most optical sensors, polarization effects are considered noise that requires correction.

Due to mirrors, gratings and prisms, the radiometric response function depends on the polarization of the incoming light. A correct radiometric calibration therefore requires knowledge of both the polarization properties of the instrument (measured before launch) and the actual polarization of the incoming light (measured for each observed pixel). Schutgens & Stammes (2002, 2003) developed the radiometric calibration methods for the polarization-sensitive spaceborne instruments for the correct retrieval of data products that require absolute radiances. Sun & Xiong (2007) analysed the MODIS visible bands sensitive to polarization of incident light.

Levy et al. (2004) demonstrated that disregarding polarization introduces little error into global and long-term averages aerosol retrieval, yet can produce very large errors on smaller scales and individual aerosol retrievals. This correction has been incorporated into the latest MODIS aerosol retrieval algorithm (Levy et al. 2007).

The polarization signature, characterized by the degree of polarization and the polarization direction, may contain some information about the surface such as its roughness (Curran 1981), water content (Curran 1978), crop types (Shibayama & Akita 2002), or the leaf inclination distribution (Rondeaux & Herman 1991, Shibayama & Watanabe 2007). Shibayama et al. (2007) linked the polarization of reflected light from crop canopies measured in the field with the leaf inclination angle.

Kokhanovsky et al. (2007) inter-compared the aerosol optical thickness (AOT) at 0.55 µm retrieved using different satellite instruments and algorithms based on the analysis of backscattered solar light for a single scene over central Europe. These algorithms are based on spectral, angular or polarization signatures. Studies demonstrate the great potential of polarization signatures in estimating AOT (Hasekamp & Landgraf 2007). Kacenelenbogen et al. (2006) analysed the relationship between daily fine particle mass concentration (PM2.5) and columnar aerosol optical depth derived from POLDER.

10.7 CONCLUSIONS

Five remote sensing signatures have been evaluated in terms of their measurement, modelling and application potential. These signatures were discussed separately in this chapter, but as has been demonstrated they are used jointly in many cases. Integration of data sets from multiple sources with different signatures will continue to play a critical role in future remote sensing research. In particular, advanced data assimilation schemes (Liang & Qin 2008), evidential reasoning (e.g. Sun & Liang 2008) and bridging scaling gaps from local to biome level will be of increasing interest.

REFERENCES

Amolins, K., Zhang, Y. & Dare, P. 2007. Wavelet based image fusion techniques—An introduction, review and comparison. *ISPRS Journal of Photogrammetry and Remote Sensing* 62: 249–263.

Aplin, P. 2006. On scales and dynamics in observing the environment. *International Journal of Remote Sensing* 27: 2123–2140.

Asner, G.P., & Lobell, D.B. 2000. A biogeophysical approach for automated SWIR unmixing of soils and vegetation. *Remote Sensing of Environment* 74: 99–112.

Atkinson, P. & Emery, D. 1999. Exploring the relation between spatial structure and wavelength: Implications for sampling reflectance in the field. *International Journal of Remote Sensing* 20: 2663–2678.

Bacour, C., Jacquemoud, S., Leroy, M., Hautceur, O., Weiss, M., Prevot, L., Bruguier, N. & Chauki, H. 2002. Reliability of the estimation of vegetation characteristics by inversion of three canopy reflectance models on airborne POLDER data. *Agronomie,* 22: 555–565.

Bailey, T.C. & Gatrell, A.C. 1995. *Interactive Spatial Data Analysis*. Harlow: Longman.

Baret, F. & Buis, S. 2008. Estimating Canopy Characteristics from Remote Sensing Observations: Review of Methods and Associated Problems. In S. Liang (ed.), *Advances in Land Remote Sensing: System, Modelling, Inversion and Application, Chapter 7*: 173–201. New York: Springer.

Börner, A., Wiest, L., Keller, P., Reulke, R., Richter, R., Schaepman, M. & Schläpfer, D. 2001. SENSOR: A tool for the simulation of hyperspectral remote sensing systems. *ISPRS Journal of Photogrammetry and Remote Sensing* 55: 299–312.

Boucher, A., Seto, K.C. & Journel, A.G. 2006. A novel method for mapping land cover changes: Incorporating time and space with geostatistics. *IEEE Transactions on Geoscience and Remote Sensing* 44: 3427–3435.

Breon, F.M., Tanre, D., Lecomte, P. & Herman, M. 1995a. Polarized Reflectance of Bare Soils and Vegetation—Measurements and Models. *IEEE Transactions on Geoscience and Remote Sensing* 33: 487–499.

Breon, F.M., Tanre, D., Lecomte, P. & Herman, M. 1995b. Polarized reflectance of bare soils and vegetation: Measurements and models. *IEEE Transactions on Geoscience and Remote Sensing* 33: 487–499.

Cabral, A., De Vasconcelos, M.J.P., Pereira, J.M.C., Bartholome, E. & Mayaux, P. 2003. Multi-temporal compositing approaches for SPOT-4 VEGETATION. *International Journal of Remote Sensing* 24: 3343–3350.

Canisius, F. & Chen, J.M. 2007. Retrieving forest background reflectance in a boreal region from Multi-anglo Imaging SpectroRadiometer (MISR) data. *Remote Sensing of Environment* 107: 312–321.

Casa, R. & Jones, H.G. 2005. LAI retrieval from multiangular image classification and inversion of a ray tracing model. *Remote Sensing of Environment* 98: 414–428.

Chen, J., Jonsson, P., Tamura, M., Gu, Z.H., Matsushita, B. & Eklundh, L. 2005a. A simple method for reconstructing a highquality NDVI time-series data set based on the Savitzky-Golay filter. *Remote Sensing of Environment* 91: 332–344.

Chen, J., Zhang, M.Y., Wang, L., Shimazaki, H. & Tamura, M. 2005b. A new index for mapping lichen-dominated biological soil crusts in desert areas. *Remote Sensing of Environment* 96: 165–175.

Chen, J.M., Deng, F. & Chen, M.Z. 2006a. Locally adjusted cubic-spline capping for reconstructing seasonal trajectories of a satellite-derived surface parameter. *IEEE Transactions on Geoscience and Remote Sensing* 44: 2230–2238.

Chen, J.M., Menges, C.H. & Leblanc, S.G. 2005c. Global mapping of foliage clumping index using multi-angular satellite data. *Remote Sensing of Environment* 97: 447–457.

Chen, J.S., Lin, H., Shao, Y. & Yang, L.M. 2006b. Oblique striping removal in remote sensing imagery based on wavelet transform. *International Journal of Remote Sensing* 27: 1717–1723.

Chikhaoui, M., Bonn, F., Bokoye, A.I. & Merzouk, A. 2005. A spectral index for land degradation mapping using ASTER data: Application to a semi-arid Mediterranean catchment. *International Journal of Applied Earth Observation and Geoinformation* 7: 140–153.

Chopping, M. 2008. Terrestrial Applications of Multiangle Remote Sensing. In S. Liang (ed.), *Advances in Land Remote Sensing: System, Modelling, Inversion and Application, Chapter 5*. New York: Springer.

Chopping, M.J., Su, L.H., Laliberte, A., Rango, A., Peters, D.P.C. & Martonchik, J.V. 2006. Mapping woody plant cover in desert grasslands using canopy reflectance modelling and MISR data. *Geophysical Research Letters* 33, Art. No. L17402.

Cierniewski, J., Gdala, T. & Karnieli, A. 2004. A hemispherical-directional reflectance model as a tool for understanding image distinctions between cultivated and uncultivated bare surfaces. *Remote Sensing of Environment* 90: 505–523.

Cihlar, J. 1996. Identification of contaminated pixels in AVHRR composite images for studies of land biosphere. *Remote Sensing of Environment* 56: 149–163.

Cihlar, J., Manak, D. & Diorio, M. 1994. Evaluation of Compositing Algorithms for Avhrr Data over Land. *IEEE Transactions on Geoscience and Remote Sensing* 32: 427–437.

Cohen, W., Spies, T. & Bradshaw, G. 1990. Semivariograms of digital imagery for analysis of conifer canopy structure. *Remote Sensing of Environment* 34: 167–178.

Coll, C., Caselles, V., Galve, J.M., Valor, E., Niclos, R. & Sanchez, J.M. 2006. Evaluation of split-window and dual-angle correction methods for land surface temperature retrieval from Envisat/Advanced Along Track Scanning Radiometer (AATSR) data. *Journal of Geophysical Research-Atmospheres* 111: Art. No. D12105.

Coppin, P., Jonckheere, I., Nackaerts, K., Muys, B. & Lambin, E. 2004. Digital change detection methods in ecosystem monitoring: a review. *International Journal of Remote Sensing* 25: 1565–1596.

Cressie, N. 1993. *Statistics for Spatial Data*. New York: John Wiley and Sons, Inc.

Curran, P. 1981. The Relationship between Polarized Visible-Light and Vegetation Amount. *Remote Sensing of Environment* 11: 87–92.

Curran, P. & Atkinson, P. 1998. Geostatistics and remote sensing. *Progress in Physical Geography* 22: 61–78.

Curran, P.J. 1978. Photographic Method for Recording of Polarized Visible-Light for Soil Surface Moisture Indications. *Remote Sensing of Environment* 7: 305–322.

Curran, P.J. 1988. The semi-variogram in remote sensing: an introduction. *Remote Sensing of Environment* 3: 493–507.

Curran, P.J. 2001. Remote sensing: Using the spatial domain. *Environmental and Ecological Statistics* 8: 331–344.

De Grandi, G.D., Lee, J.S. & Schuler, D.L. 2007. Target detection and texture segmentation in polarimetric SAR images using a wavelet frame: Theoretical aspects. *IEEE Transactions on Geoscience and Remote Sensing* 45: 3437–3453.

Deuze, J.L., Breon, F.M., Deschamps, P.Y., Devaux, C., Herman, M., Podaire, A. & Roujean, J.L. 1993. Analysis of the Polder (Polarization and Directionality of Earths Reflectances) Airborne Instrument Observations over Land Surfaces. *Remote Sensing of Environment* 45: 137–154.

Diner, D.J., Martonchik, J.V., Kahn, R.A., Pinty, B., Gobron, N., Nelson, D.L. & Holben, B.N. 2005. Using angular and spectral shape similarity constraints to improve MISR aerosol and surface retrievals over land. *Remote Sensing of Environment* 94: 155–171.

Disney, M., Lewis, P. & Saich, P. 2006. 3D modelling of forest canopy structure for remote sensing simulations in the optical and microwave domains. *Remote Sensing of Environment* 100: 114–132.

Dorigo, W.A., Zurita-Milla, R., de Wit, A.J.W., Brazile, J., Singh, R. & Schaepman, M.E. 2007. A review on reflective remote sensing and data assimilation techniques for enhanced agroecosystem modelling. *International Journal of Applied Earth Observation and Geoinformation* 9: 165–193.

Durbha, S.S., King, R.L. & Younan, N.H. 2007. Support vector machines regression for retrieval of leaf area index from multiangle imaging spectroradiometer. *Remote Sensing of Environment* 107: 348–361.

Egan, W.G., Johnson, W.R. & Whitehead, V.S. 1991. Terrestrial Polarization Imagery Obtained from the Space—Shuttle—Characterization and Interpretation. *Applied Optics* 30: 435–442.

Eismann, M.T. & Hardie, R.C. 2004. Application of the stochastic mixing model to hyperspectral resolution, enhancement. *IEEE Transactions on Geoscience and Remote Sensing* 42: 1924–1933.

Eismann, M.T. & Hardie, R.C. 2005. Hyperspectral resolution enhancement using high-resolution multispectral imagery with arbitrary response functions. *IEEE Transactions on Geoscience and Remote Sensing* 43: 455–465.

Fang, H., Kim, H., Liang, S., Schaaf, C., Strahler, A., Townshend, G.R.G. & Dickinson, R. 2007. Spatially and temporally continuous land surface albedo fields and validation. *Journal of Geophysical Research-Atmosphere, 112, Article Number* D20206, doi:20210.21029/22006JD008377.

Fang, H. & Liang, S. 2003. Retrieve LAI from Landsat 7 ETM+ Data with a Neural Network Method: Simulation and Validation Study. *IEEE Transactions on Geoscience and Remote Sensing* 41: 2052–2062.

Fang, H. & Liang, S. 2005. A hybrid inversion method for mapping leaf area index from MODIS data: experiments and application to broadleaf and needleleaf canopies. *Remote Sensing of Environment* 94: 405–424.

Fang, H., Liang, S. & Kuusk, A. 2003. Retrieving Leaf Area Index (LAI) Using a Genetic Algorithm with a Canopy Radiative Transfer Model. *Remote Sensing of Environment* 85: 257–270.

Fang, H., Liang, S., Townshend, J. & Dickinson, R. 2008. Spatially and temporally continuous LAI data sets based on a new filtering method: Examples from North America. *Remote Sensing of Environment* 112: 75–93.

Fischer, A. 1994b. A simple model for the temporal variations of NDVI at regional scale over agricultural countries.

Validation with ground radiometric measurements. *International Journal of Remote Sensing* 15: 1421–1446.

Fisher, A. 1994a. A model for the seasonal variations of vegetation indices in coarse resolution data and its inversion to extract crop parameters. *Remote Sensing of Environment* 48: 220–230.

Franklin, J. & Turner, D.L. 1992. The application of a geometric optical canopy reflectance model to semiarid shrub vegetation. *IEEE Transactions on Geoscience and Remote Sensing* 30: 293–301.

Garcia-Haro, F.J., Camacho-de Coca, F. & Melia, J. 2006. A directional spectral mixture analysis method: Application to multiangular airborne measurements. *IEEE Transactions on Geoscience and Remote Sensing* 44: 365–377.

Garcia-Haro, F.J., Sommer, S. & Kemper, T. 2005. A new tool for variable multiple endmember spectral mixture analysis (VMESMA. *International Journal of Remote Sensing* 26: 2135–2162.

Gascon, F., Gastellu-Etchegorry, J.P., Lefevre-Fonollosa, M.J. & Dufrene, E. 2004. Retrieval of forest biophysical variables by inverting a 3-D radiative transfer model and using high and very high resolution imagery. *International Journal of Remote Sensing* 25: 5601–5616.

Gastellu-Etchegorry, J.P., Gascon, F. & Esteve, P. 2003. An interpolation procedure for generalizing a look-up table inversion method. *Remote Sensing of Environment* 87: 55–71.

Gerstl, S.A.W. 1990. Physics concepts of optical and radar reflectance signatures A summary review. *International Journal of Remote Sensing* 11: 1109–1117.

Gitelson, A.A., Gritz, Y. & Merzlyak, M.N. 2003. Relationships between leaf chlorophyll content and spectral reflectance and algorithms for non-destructive chlorophyll assessment in higher plant leaves. *Journal of Plant Physiology* 160: 271–282.

Goovaerts, P. 1997. *Geostatistics for Natural Resources Evaluation*. New York: Oxford University Press.

Govaerts, Y.M. & Lattanzio, A. 2007. Retrieval error estimation of surface albedo derived from geostationary large band satellite observations: Application to Meteosat-2 and Meteosat-7 data. *Journal of Geophysical Research-Atmospheres* 112, Art. No. D05102.

Govaerts, Y.M., Lattanzio, A., Pinty, B. & Schmetz, J. 2004. Consistent surface albedo retrieval from two adjacent geostationary satellites. *Geophysical Research Letters* 31, Art. No. L15201.

Grey, W.M.F., North, P.R.J., Los, S.O. & Mitchell, R.M. 2006. Aerosol Optical Depth and Land Surface Reflectance from Multi-angle AATSR Measurements: Global Validation and Inter-sensor Comparisons. *IEEE Transactions on Geoscience and Remote Sensing* 44: 2184–2197.

Gross, H.N. & Schott, J.R. 1998. Application of spectral mixture analysis and image fusion techniques for image sharpening. *Remote Sensing of Environment* 63: 85–94.

Hansen, M., DeFries, R.S., Townshend, J.R.G., Sohlberg, R., Dimiceli, C. & Carroll, M. 2002. Towards an operational MODIS continuous field of percent tree cover algorithm: Examples using AVHRR and MODIS data. *Remote Sensing of Environment* 83: 303–319.

Harris, A., Bryant, R.G. & Baird, A.J. 2005. Detecting near-surface moisture stress in Sphagnum spp. *Remote Sensing of Environment* 97: 371–381.

Hasekamp, O.P. & Landgraf, J. 2007. Retrieval of aerosol properties over land surfaces: capabilities of multiple-viewing-angle intensity and polarization measurements. *Applied Optics* 46: 3332–3344.

Herman, M. & Vanderbilt, V. 1997. Polarimetric observations in the solar spectrum for remote sensing purposes. *Remote Sensing Reviews* 15: 35–57.

Hermance, J.F. 2007. Stabilizing high-order, non-classical harmonic analysis of NDVI data for average annual models by damping model roughness. *International Journal of Remote Sensing* 28: 2801–2819.

Hermance, J.F., Jacob, R.W., Bradley, B.A. & Mustard, J.F. 2007. Extracting phenological signals from multi-year AVHRR NDVI time series: Framework for applying high-order annual splines with roughness damping. *IEEE Transactions on Geoscience and Remote Sensing* 45: 3264–3276.

Holben, B.N. 1986. Characteristics of maximum-value composite images for temporal AVHRR data. *International Journal of Remote Sensing* 7: 1435–1445.

Hsu, N.C., Tsay, S.C., King, M.D. & Herman, J.R. 2004. Aerosol properties over bright-reflecting source regions. *IEEE Transactions on Geoscience and Remote Sensing* 42: 557–569.

Jackson, T. 2008. Passive Microwave Remote Sensing for Land Applications. In S. Liang (ed.), *Advances in Land Remote Sensing: System, Modelling, Inversion and Application, Chapter 2*: 9–18. New York: Springer.

Jimenez-Munoz, J.C. & Sobrino, J.A. 2007. Feasibility of retrieving land-surface temperature from ASTER TIR bands using two-channel algorithms: A case study of agricultural areas. *IEEE Geoscience and Remote Sensing Letters* 4: 60–64.

Jobanputra, R. & Clausi, D.A. 2006. Preserving boundaries for image texture segmentation using grey level co-occurring probabilities. *Pattern Recognition* 39: 234–245.

Jonsson, P. & Eklundh, L. 2002. Seasonality extraction by function fitting to time—series of satellite sensor data. *IEEE Transactions on Geoscience and Remote Sensing* 40: 1824–1832.

Jonsson, P. & Eklundh, L. 2004. TIMESAT—a program for analyzing time-series of satellite sensor data. *Computers and Geosciences* 30: 833–845.

Julien, Y., Sobrino, J.A. & Verhoef, W. 2006. Changes in land surface temperatures and NDVI values over Europe between 1982 and 1999. *Remote Sensing of Environment* 103: 43–55.

Jupp, D.L.B., Strahler, A.H. & Woodcock, C.E. 1988. Autocorrelation and regularization in digital images I. Basic theory. *IEEE Transactions on Geoscience and Remote Sensing* 26: 463–473.

Jupp, D.L.B., Strahler, A.H. & Woodcock, C.E. 1989. Autocorrelation and regularization in digital images II. Simple image models. *IEEE Transactions on Geoscience and Remote Sensing* 27: 247–258.

Kacenelenbogen, M., Leon, J.F., Chiapello, I. & Tanre, D. 2006. Characterization of aerosol pollution events in France using ground-based and POLDER-2 satellite data. *Atmospheric Chemistry and Physics* 6: 4843–4849.

Kalacska, M., Sanchez-Azofeifa, A., Caelli, T., Rivard, B. & Boerlage, B. 2005. Estimating leaf area index from satellite imagery using Bayesian networks. *IEEE Transactions on Geoscience and Remote Sensing* 43: 1866–1873.

Kandaswamy, U., Adjeroh, D.A. & Lee, A.C. 2005. Efficient texture analysis of SAR imagery. *IEEE Transactions on Geoscience and Remote Sensing* 43: 2075–2083.

Kayitakire, F., Hamel, C. & Defourny, P. 2006. Retrieving forest structure variables based on image texture analysis and IKONOS-2 imagery. *Remote Sensing of Environment* 102: 390–401.

Kimes, D., Gastellu-Etchegorry, J. & Esteve, P. 2002. Recovery of forest canopy characteristics through inversion of a complex 3D model. *Remote Sensing of Environment* 79: 320–328.

Kimes, D.S., Ranson, K.J., Sun, G. & Blair, J.B. 2006. Predicting lidar measured forest vertical structure from multi-angle spectral data. *Remote Sensing of Environment* 100: 503–511.

Kneubühler, M., Koetz, B., Huber, S., Schopfer, J., Richter, R. and Itten, K.I. 2006. Monitoring vegetation growth using multitemporal CHRIS/PROBA data. *IEEE Geoscience and Remote Sensing Symposium (IGARSS 2006)*: 2677–2680. IEEE Denver (USA).

Kobayashi, H., Suzuki, R. & Kobayashi, S. 2007. Reflectance seasonality and its relation to the canopy leaf area index in an eastern Siberian larch forest: Multi-satellite data and radiative transfer analyses. *Remote Sensing of Environment* 106: 238–252.

Koetz, B., Baret, F., Poilve, H. & Hill, J. 2005. Use of coupled canopy structure dynamic and radiative transfer models to estimate biophysical canopy characteristics. *Remote Sensing of Environment* 95: 115–124.

Koetz, B., Kneubühler, M., Huber, S., Schopfer, J. and Baret, F. 2007. Radiative transfer model inversion based on multi-temporal CHRIS/PROBA data for LAI estimation. In M.E. Schaepman, S. Liang, N.E. Groot & M. Kneubühler (eds.), *10th Intl. Symposium on Physical Measurements and Spectral Signatures in Remote Sensing, Intl. Archives of the Photogrammetry, Remote Sensing and Spatial Information Sciences* XXXVI, Part 7/C50, 344–349. ISSN 1682-1777.

Kokhanovsky, A.A., Aoki, T., Hachikubo, A., Hori, M. & Zege, E.P. 2005. Reflective properties of natural snow: Approximate asymptotic theory versus in situ measurements. *IEEE Transactions on Geoscience and Remote Sensing* 43: 1529–1535.

Kokhanovsky, A.A., Breon, F.M., Cacciari, A., Carboni, E., Diner, D., Di Nicolantonio, W., Grainger, R.G., Grey, W.M.F., Holler, R., Lee, K.H., Li, Z., North, P.R.J., Sayer, A.M., Thomas, G.E. & von Hoyningen-Huene, W. 2007. Aerosol remote sensing over land: A comparison of satellite retrievals using different algorithms and instruments. *Atmospheric Research* 85: 372–394.

Kotchenova, S.Y., Shabanov, N.V., Knyazikhin, Y., Davis, A.B., Dubayah, R. & Myneni, R.B. 2003. Modelling lidar waveforms with time-dependent stochastic radiative transfer theory for remote estimations of forest structure. *Journal of Geophysical Research-Atmospheres* 108, Art. No. 4484.

Kotchenova, S.Y. & Vermote, E.F. 2007. Validation of a vector version of the 6S radiative transfer code for atmospheric correction of satellite data. Part II. Homogeneous Lambertian and anisotropic surfaces. *Applied Optics* 46: 4455–4464.

Kotchenova, S.Y., Vermote, E.F., Matarrese, R. & Klemm, F.J. 2006. Validation of a vector version of the 6S radiative transfer code for atmospheric correction of satellite data. Part I: Path radiance. *Applied Optics* 45: 6762–6774.

Kuusk, A. 1998. Monitoring of vegetation parameters on large areas by the inversion of a canopy reflectance model. *International Journal of Remote Sensing* 19: 2893–2905.

Lam, N. 2008. Methodologies for Mapping Land Cover/ Land Use and its Change. In S. Liang (ed.), *Advances in Land Remote Sensing: System, Modelling, Inversion and Application, Chapter 13*: 341–367. New York: Springer.

Levy, R.C., Remer, L.A. & Kaufman, Y.J. 2004. Effects of neglecting polarization on the MODIS aerosol retrieval over land. *IEEE Transactions on Geoscience and Remote Sensing* 42: 2576–2583.

Levy, R.C., Remer, L.A., Mattoo, S., Vermote, E.F. & Kaufman, Y.J. 2007. Second-generation operational algorithm: Retrieval of aerosol properties over land from inversion of Moderate Resolution Imaging Spectroradiometer spectral reflectance. *Journal of Geophysical Research-Atmospheres* 112.

Li, B., Jiao, R.H. & Li, Y.C. 2007. Fast adaptive wavelet for remote sensing image compression. *Journal of Computer Science and Technology* 22: 770–778.

Li, S.S. & Zhou, X.B. 2004. Modelling and measuring the spectral bidirectional reflectance factor of snow-covered sea ice: An intercomparison study. *Hydrological Processes* 18: 3559–3581.

Liang, S. 2001. Land cover classification methods for multi-year AVHRR data. *International Journal of Remote Sensing* 22: 1479–1493.

Liang, S. 2004. *Quantitative Remote Sensing of Land Surfaces*. New York: John Wiley and Sons, Inc.

Liang, S., Fallah-Adl, H., Kalluri, S., JaJa, J., Kaufman, Y.J. & Townshend, J.R.G. 1997. An operational atmospheric correction algorithm for Landsat Thematic Mapper imagery over the land. *Journal of Geophysical Research-Atmospheres* 102: 17173–17186.

Liang, S. & Fang, H. 2004. An improved atmospheric correction algorithm for hyperspectral remotely sensed imagery. *IEEE Geoscience and Remote Sensing Letters* 1: 112–117.

Liang, S. & Strahler, A. 2000. Land surface Bidirectional Reflectance Distribution Function (BRDF): Recent advances and future prospects. *Remote Sensing Reviews* 18: 83–551.

Liang, S. & Qin, J. 2008. Data assimilation methods for land surface variable estimation. In S. Liang (ed.), *Advances in Land Remote Sensing: System, Modelling, Inversion and Application*: 313–339. New York: Springer.

Liang, S., Zheng, T., Liu, R., Fang, H., Tsay, S.C. & Running, S. 2006a. Mapping incident Photosynthetically Active Radiation (PAR) from MODIS Data. *Journal of Geophysical Research-Atmospheres* 111, D15208, doi:15210.11029/12005JD006730.

Liang, S., Zhong, B. & Fang, H. 2006b. Improved estimation of aerosol optical depth from MODIS imagery over land surfaces. *Remote Sensing of Environment* 104: 416–425.

Liang, S.L., Stroeve, J. & Box, J.E. 2005. Mapping daily snow/ice shortwave broadband albedo from Moderate Resolution Imaging Spectroradiometer (MODIS): The improved direct retrieval algorithm and validation with

Greenland *in situ* measurement. *Journal of Geophysical Research-Atmospheres* 110, Art. No. D10109.

Liang, S.L., Zheng, T., Wang, D.D., Wang, K.C., Liu, R.G., Tsay, S.C., Running, S. & Townshend, J. 2007. Mapping high-resolution incident photosynthetically active radiation over land from polar–orbiting and geostationary satellite data. *Photogrammetric Engineering and Remote Sensing* 73: 1085–1089.

Liangrocapart, S. & Petrou, M. 2002. A two-layer model of the bidirectional reflectance of homogeneous vegetation canopies. *Remote Sensing of Environment* 80: 17–35.

Liu, J.C., Melloh, R.A., Woodcock, C.E., Davis, R.E. & Ochs, E.S. 2004. The effect of viewing geometry and topography on viewable gap fractions through forest canopies. *Hydrological Processes* 18: 3595–3607.

Liu, X.H., Clarke, K. & Herold, M. 2006. Population density and image texture: A comparison study. *Photogrammetric Engineering and Remote Sensing* 72: 187–196.

Lu, X., Liu, R., Liu, J. & Liang, S. 2007. Removal of Noise by Wavelet Method to Generate High Quality Temporal Data of Terrestrial MODIS Products. *Photogrammetric Engineering and Remote Sensing* 73: 1129–1139.

Luo, J., Ming, D., Shen, Z., Wang, M. & Sheng, H. 2007. Multi-scale information extraction from high resolution remote sensing imagery and region partition methods based on GMRF-SVM. *International Journal of Remote Sensing* 28: 3395–3412.

Magnussen, S., Naesset, E. & Wulder, M.A. 2007. Efficient multiresolution spatial predictions for large data arrays. *Remote Sensing of Environment* 109: 451–463.

Malenovsky, Z., Martin, E., Homolova, L., Gastellu-Etchegory, J.P., Zurita-Milla, R., Schaepman, M.E., Pokorny, R., Clevers, J.G.P.W. & Cudlin, P. 2008. Influence of woody elements of a Norway spruce canopy on nadir reflectance simulated by the DART model at very high spatial resolution. *Remote Sensing of Environment* 112: 1–18.

Martonchik, J.V., Diner, D.J., Crean, K.A. & Bull, M.A. 2002. Regional Aerosol Retrieval Results From MISR. *IEEE Transactions on Geoscience and Remote Sensing* 40: 1520–1531.

Meher, S.K., Shankar, B.U. & Ghosh, A. 2007. Wavelet-feature-based classifiers for multispectral remote sensing images. *IEEE Transactions on Geoscience and Remote Sensing* 45: 1881–1886.

Menenti, M., Jia, L. & Li, Z.L. 2008. Multi–angular Thermal Infrared Observations of Terrestrial Vegetation. In S. Liang (ed.), *Advances in Land Remote Sensing: System, Modelling, Inversion and Application, Chapter 4*: 51–93. New York: Springer.

Meroni, M., Colombo, R. & Panigada, C. 2004. Inversion of a radiative transfer model with hyperspectral observations for LAI mapping in poplar plantations. *Remote Sensing of Environment* 92: 195–206.

Mertens, K.C., Verbeke, L.P.C., Ducheyne, E.I. & De Wulf, R.R. 2003. Using genetic algorithms in sub-pixel mapping. *International Journal of Remote Sensing* 24: 4241–4247.

Mertens, K.C., Verbeke, L.P.C., Westra, T. & De Wulf, R.R. 2004. Sub-pixel mapping and sub-pixel sharpening using neural network predicted wavelet coefficients. *Remote Sensing of Environment* 91: 225–236.

Miesch, C., Poutier, L., Achard, W., Briottet, X., Lenot, X. & Boucher, Y. 2005. Direct and inverse radiative transfer solutions for visible and near-infrared hyperspectral imagery. *IEEE Transactions on Geoscience and Remote Sensing* 43: 1552–1562.

Moody, A. & Johnson, D.M. 2001. Land-surface phenologies from AVHRR using the discrete fourier transform. *Remote Sensing of Environment* 75: 305–323.

Moody, E.G., King, M.D., Platnick, S., Schaaf, C.B. & Gao, F. 2005. Spatially complete global spectral surface albedos: Value-added datasets derived from terra MODIS land products. *IEEE Transactions on Geoscience and Remote Sensing* 43: 144–158.

Myint, S.W. & Lam, N. 2005. Examining lacunarity approaches in comparison with fractal and spatial autocorrelation techniques for urban mapping. *Photogrammetric Engineering and Remote Sensing* 71: 927–937.

Myint, S.W., Lam, N.S.N. & Tyler, J.M. 2004. Wavelets for urban spatial feature discrimination: Comparisons with fractal, spatial autocorrelation & spatial co-occurrence approaches. *Photogrammetric Engineering and Remote Sensing* 70: 803–812.

Nadal, F. & Breon, F.M. 1999. Parameterization of surface polarized reflectance derived from POLDER spaceborne measurements. *IEEE Transactions on Geoscience and Remote Sensing* 37: 1709–1718.

Nilson, T., Kuusk, A., Lang, M. & Lukk, T. 2003. Forest reflectance modelling: Theoretical aspects and applications. *Ambio* 32: 535–541.

North, P.R.J. 2002. Estimation of f(APAR), LAI & vegetation fractional cover from ATSR-2 imagery. *Remote Sensing of Environment* 80: 114–121.

Oku, Y. & Ishikawa, H. 2004. Estimation of land surface temperature over the Tibetan Plateau using GMS data. *Journal of Applied Meteorology* 43: 548–561.

Peddle, D.R., Franklin, S.E., Johnson, R.L., Lavigne, M.B. & Wulder, M.A. 2003. Structural change detection in a disturbed conifer forest using a geometric optical reflectance model in multiple-forward mode. *IEEE Transactions on Geoscience and Remote Sensing* 41: 163–166.

Peddle, D.R., Johnson, R.L., Cihlar, J. & Latifovic, R. 2004. Large area forest classification and biophysical parameter estimation using the 5-Scale canopy reflectance model in multiple forward-mode. *Remote Sensing of Environment* 89: 252–263.

Phinn, S., Franklin, J., Hope, A., Stow, D. & Huenneke, L. 1996. Biomass distribution mapping using airborne digital video imagery and spatial statistics in a semi-arid environment. *Journal of Environmental Management* 47: 139–164.

Pinker, R.T., Li, X., Meng, W. & Yegorova, E.A. 2007. Toward improved satellite estimates of short-wave radiative fluxes—Focus on cloud detection over snow: 2. Results. *Journal of Geophysical Research-Atmospheres* 112.

Pinty, B., Gobron, N., Widlowski, J.L., Lavergne, T. & Verstraete, M.M. 2004a. Synergy between 1-D and 3-D radiation transfer models to retrieve vegetation canopy properties from remote sensing data. *Journal of Geophysical Research-Atmospheres* 109, Art. No. D21205 .

Pinty, B., Widlowski, J.L., Taberner, M., Gobron, N., Verstraete, M.M., Disney, M., Gascon, F., Gastellu, J.P., Jiang, L., Kuusk, A., Lewis, P., Li, X., Ni-Meister, W., Nilson, T., North, P., Qin, W., Su, L., Tang, S., Thompson, R., Verhoef, W., Wang, H., Wang, J., Yan, G. & Zang, H. 2004b. Radiation Transfer Model Intercom-

parison (RAMI) exercise: Results from the second phase. *Journal of Geophysical Research-Atmospheres* 109, Art. No. D06210, ISI:000220622400004.

Pitman, K.M., Wolff, M.J. & Clayton, G.C. 2005. Application of modern radiative transfer tools to model laboratory quartz emissivity. *Journal of Geophysical Research-Planets* 110, Art. No. E08003.

Pohl, C. & van Genderen, J.L. 1998. Multisensor image fusion in remote sensing: concepts, methods and applications. *International Journal of Remote Sensing* 19: 823–854.

Purkis, S.J., Myint, S.W. & Riegl, B.M. 2006. Enhanced detection of the coral Acropora cervicornis from satellite imagery using a textural operator. *Remote Sensing of Environment* 101: 82–94.

Qi, J. & Kerr, Y. 1997. On current compositing algorithms. *Remote Sensing Reviews* 15: 235–256.

Qi, J., Kerr, Y.H., Moran, M.S., Weltz, M., Huete, A.R., Sorooshian, S. & Bryant, R. 2000. Leaf area index estimates using remotely sensed data and BRDF models in a semiarid region. *Remote Sensing of Environment* 73: 18–30.

Qin, J., Liang, S., Li, X. & Wang, J. 2007. Development of the adjoint model of a canopy radiative transfer model for sensivity study and inversion of leaf area index. *IEEE Transactions on Geoscience and Remote Sensing*, revised.

Ramstein, G. & Raffy, M. 1989. Analysis of the structure of radiometric remotely sensed images. *International Journal of Remote Sensing* 10: 1049–1073.

Ranchin, T., Aiazzi, B., Alparone, L., Baronti, S. & Wald, L. 2003. Image fusion—the ARSIS concept and some successful implementation schemes. *ISPRS Journal of Photogrammetry and Remote Sensing* 58: 4–18.

Rautiainen, M. & Stenberg, P. 2005. Application of photon recollision probability in coniferous canopy reflectance simulations. *Remote Sensing of Environment* 96: 98–107.

Roerink, G.J., Menenti, M. & Verhoef, W. 2000. Reconstructing cloudfree NDVI composites using Fourier analysis of time series. *International Jour. of Remote Sensing* 21: 1911–1917.

Roger, J.C., Santer, R., Herman, M. & Deuze, J.L. 1994. Polarization of the Solar Light Scattered by the Earth Atmosphere System as Observed from the United States. Shuttle. *Remote Sensing of Environment* 48: 275–290

Rondeaux, G. & Herman, M. 1991. Polarization of light reflected by crop canopies. *Remote Sensing of Environment* 38: 63–75.

Roujean, J.-L. & Breon, F.-M. 1995. Estimating PAR absorbed by vegetation from bidirectional reflectance measurements. *Remote Sensing of Environment* 51: 375–384.

Roujean, J.L. & Lacaze, R. 2002. Global mapping of vegetation parameters from POLDER multiangular measurements for studies of surface-atmosphere interactions: A pragmatic method and its validation. *Journal of Geophysical Research-Atmospheres,* 107.

Salomonson, V.V. & Appel, I. 2004. Estimating fractional snow cover from MODIS using the normalized difference snow index. *Remote Sensing of Environment* 89: 351–360.

Schaaf, C., Martonchik, J., Pinty, B., Govaerts, Y., Gao, F., Lattanzio, A., Liu, J., Strahler, A. & Taberner, M. 2008. Retrieval of Surface Albedo from Satellite Sensors. In S. Liang (ed.), *Advances in Land Remote Sensing: System, Modelling, Inversion and Application, Chapter 9*: 219–243. New York: Springer.

Schaepman-Strub, G., Schaepman, M.E., Painter, T.H., Dangel, S. & Martonchik, J.V. 2006. Reflectance quantities in optical remote sensing—definitions and case studies. *Remote Sensing of Environment* 103: 27–42.

Schaepman, M.E. 2007. Spectrodirectional Remote Sensing: From Pixels to Processes. *International Journal of Applied Earth Observation and Geoinformation* 9: 204–223.

Schaepman, M.E., Koetz, B., Schaepman-Strub, G. & Itten, K.I. 2005. Spectrodirectional remote sensing for the improved estimation of biophysical and chemical variables: Two case studies. *International Journal of Applied Earth Observation and Geoinformation* 6: 271–282.

Schlerf, M., Atzberger, C. & Hill, J. 2005. Remote sensing of forest biophysical variables using HyMap imaging spectrometer data. *Remote Sensing of Environment* 95: 177–194.

Schmidt, F., Doute, S. & Schmitt, B. 2007. WAVANGLET: An efficient supervised classifier for hyperspectral images. *IEEE Transactions on Geoscience and Remote Sensing* 45: 1374–1385

Schutgens, N.A.J. & Stammes, P. 2002. Parametrisation of Earth's polarisation spectrum in the ultra-violet. *Jour. of Quantitative Spectroscopy and Radiative Transfer* 75: 239–255.

Schutgens, N.A.J. & Stammes, P. 2003. A novel approach to the polarization correction of spaceborne spectrometers. *Journal of Geophysical Research-Atmospheres,* 108, NO. D7, 4229, doi:10.1029/2002JD002736.

Sellers, P., Tucker, C., Collatz, G., Los, S., Justice, C., Dazlich, D. & Randall, D. 1994. A global 1 by 1 NDVI data set for climate studies. Part 2: The generation of global fields of terrestrial biophysical parameters from the NDVI. *International Journal of Remote Sensing* 15: 3519–3546.

Shabanov, N.V., Huang, D., Yang, W., Tian, B., Knyazikhin, Y., Myneni, R.B., Ahl, D.E., Gower, S.T., Huete, A.R., Arogao, L.E.O.C. & Shimabukuro, Y.E. 2005. Analysis and optimization of the MODIS leaf area index algorithm retrievals over broadleaf forests. *IEEE Transactions on Geoscience and Remote Sensing* 43: 1855–1865.

Shi, J. 2008. Active Microwave Remote Sensing Systems and Applications to Snow Monitoring. In S. Liang (ed.), *Advances in Land Remote Sensing: System, Modelling, Inversion and Application, Chapter 3*: 19–49. New York: Springer.

Shibayama, M. & Akita, S. 2002. A Portable Spectropolarimeter for field crop canopies—Distinguishing species and cultivars of fully developed canopies by polarized light. *Plant Production Science* 5: 311–319.

Shibayama, M. & Watanabe, Y. 2007. Estimating the mean leaf inclination angle of wheat canopies using reflected polarized light. *Plant Production Science* 10: 329–342.

Smolander, S. & Stenberg, P. 2003. A method to account for shoot scale clumping in coniferous canopy reflectance models. *Remote Sensing of Environment* 88: 363–373.

Sobrino, J.A., Soria, G. & Prata, A.J. 2004. Surface temperature retrieval from Along Track Scanning Radiometer 2 data: Algorithms and validation. *Journal of Geophysical Research-Atmospheres* 109, Art. No. D11101.

Soenen, S.A., Peddle, D.R. & Coburn, C.A. 2005. SCS + C: A modified sun-canopy-sensor topographic correction in forested terrain. *IEEE Transactions on Geoscience and Remote Sensing* 43: 2148–2159.

St-Onge, B.A. & Cavayas, F. 1995. Estimating forest stand structure from high resolution imagery using the directional variogram. *International Journal of Remote Sensing* 16: 1999–2021.

Sun, D.L., Pinker, R.T. & Basara, J.B. 2004. Land surface temperature estimation from the next generation of Geostationary Operational Environmental Satellites: GOES M-Q. *Journal of Applied Meteorology* 43: 363–372.

Sun, J.Q. & Xiong, X.X. 2007. MODIS polarization—sensitivity analysis. *IEEE Transactions on Geoscience and Remote Sensing* 45: 2875–2885.

Sun, W. & Liang, S. 2008. Methodologies for mapping plant functional types. In S. Liang (ed.), *Advances in Land Remote Sensing: System, Modelling, Inversion and Application*: 369–393. New York: Springer.

Talmage, D.A. & Curran, P.J. 1986. Remote Sensing Using Partially Polarized Light. *International Journal of Remote Sensing* 7: 47–64.

Tang, J., Wang, L. & Yao, Z. 2007. Spatio-temporal urban landscape change analysis using the Markov chain model and a modified genetic algorithm. *International Journal of Remote Sensing* 28: 3255–3271.

Tyo, J.S., Goldstein, D.L., Chenault, D.B. & Shaw, J.A. 2006. Review of passive imaging polarimetry for remote sensing applications. *Applied Optics* 45: 5453–5469.

Unsalan, C. 2007. Measuring land development in urban regions using graph theoretical and conditional statistical features. *IEEE Transactions on Geoscience and Remote Sensing* 45: 3989–3999.

Ustin, S., Asner, G., Gamon, J., Huemmerich, K., Jacquemoud, S., Zarco-Tejada, P. & Schaepman, M.E. 2008. Retrieval of Quantitative and Qualitative Information about Plant Pigment Systems from High Resolution Spectroscopy. *Remote Sensing of Environment.*

Vanderbilt, V.C. & Grant, L. 1985. Plant canopy specular reflectance model. *IEEE Transactions on Geoscience and Remote Sensing* 23: 722–730.

Verrelst, J., Schaepman, M.E., Kötz, B. & Kneubühler, M. 2008. Angular sensitivity of vegetation indices derived from CHRIS/PROBA data in two Alpine eco-systems. *Remote Sensing of Environment*, in press.

Vesteinsson, A., Aanaes, H., Sveinsson, J.R. & Benediktsson, J.A. 2008. Spectrally Consistent Pansharpening. In S. Liang (ed.), *Advances in Land Remote Sensing: System, Modelling, Inversion and Application*, *Chapter 11*: 293–311. New York: Springer.

Viovy, N., Arino, O. & Belward, A.S. 1992. The Best Index Slope Extraction (Bise)—a Method for Reducing Noise in Ndvi Time-Series. *International Journal of Remote Sensing* 13: 1585–1590.

Wang, K., Liang, S., Zheng, T. & Wang, D. 2007. Simultaneous estimation of surface photosynthetically active radiation and albedo from GOES. *Remote Sensing of Environment*, revised.

Widlowski, J.L., Pinty, B., Gobron, N., Verstraete, M.M., Diner, D.J. & Davis, A.B. 2004. Canopy structure parameters derived from multi-angular remote sensing data for terrestrial carbon studies. *Climatic Change* 67: 403–415.

Widlowski, J.L., Pinty, B., Lavergne, T., Verstraete, M.M. & Gobron, N. 2005. Using 1-D models to interpret the reflectance anisotropy of 3-D canopy targets: Issues and caveats. *IEEE Transactions on Geoscience and Remote Sensing* 43: 2008–2017.

Widlowski, J.L., Taberner, M., Pinty, B., Bruniquel-Pinel, V., Disney, M., Fernandes, R., Gastellu-Etchegorry, J.P., Gobron, N., Kuusk, A., Lavergne, T., Leblanc, S., Lewis, P.E., Martin, E., Mottus, M., North, P.R.J., Qin, W., Robustelli, M., Rochdi, N., Ruiloba, R., Soler, C., Thompson, R., Verhoef, W., Verstraete, M.M. & Xie, D. 2007. Third Radiation Transfer Model Intercomparison (RAMI) exercise: Documenting progress in canopy reflectance models. *Journal of Geophysical Research-Atmospheres* 112, Art. No. D09111.

Woodcock, C.E. & Strahler, A.H. 1987. The factor of scale in remote sensing. *Remote Sensing of Environment* 21: 311–332.

Woodcock, C.E., Strahler, A.H. & Jupp, D.L.B. 1988a. The use of variograms in remote sensing: Part I. Scene models and simulated images. *Remote Sensing of Environment* 25: 323–348.

Woodcock, C.E., Strahler, A.H. & Jupp, D.L.B. 1988b. The use of variograms in remote sensing: Part II. Real digital images. *Remote Sensing of Environment* 25: 349–379.

Xia, Y., Feng, D. & Zhao, R.C. 2006. Adaptive segmentation of textured images by using the coupled Markov random field model. *IEEE Transactions on Image Processing* 15: 3559–3566.

Xiao, X.M., Braswell, B., Zhang, Q.Y., Boles, S., Frolking, S. & Moore, B. 2003. Sensitivity of vegetation indices to atmospheric aerosols: continental—scale observations in Northern Asia. *Remote Sensing of Environment* 84: 385–392.

Zeng, Y., Huang, J., Wu, B., Schaepman, M.E., de Bruin, S. & Clevers, J. 2008a. Comparison of two canopy reflectance models inversion for mapping forest crown closure using imaging spectroscopy. *Canadian J. of Rem Sens* (in press).

Zeng, Y., Schaepman, M.E., Wu, B., Clevers, J.G.P.W. & Bregt, A. 2008b. Quantitative forest canopy structure assessment using an inverted geometric-optical model and up-scaling. *International Journal of Remote Sensing*, in press.

Zhang, Q., Wang, J., Gong, P. & Shi, P. 2003. Study of urban spatial patterns from SPOT panchromatic imagery using textural analysis. *International Journal of Remote Sensing* 24: 4137–4160.

Zhang, Y., Tian, Y., Knyazikhin, Y., Martonchik, J.V., Diner, D.J., Leroy, M. & Myneni, R.B. 2000. Prototyping of MISR LAI and FPAR algorithm with POLDER data over Africa. *IEEE Transactions on Geoscience and Remote Sensing* 38: 2402–2418.

Zheng, T., Liang, S. & Wang, K.C. 2007. Estimation of incident PAR from GOES imagery. *Journal of Applied Meteorology and Climatology*, in press.

Zhong, B., Liang, S. & Holben, B. 2007. Validating a new algorithm for estimating aerosol optical depths from MODIS imagery. *International Journal of Remote Sensing* 28: 4207–4214.

Zhong, P. & Wang, R.S. 2007. A multiple conditional random fields ensemble model for urban area detection in remote sensing optical Images. *IEEE Transactions on Geoscience and Remote Sensing* 45: 3978–3988.